A numerical study on the performance of the point absorber Wave Energy Converter integrated with an adjustable draft system

Tan, Jian; Polinder, Henk; Laguna, Antonio Jarquin; Miedema, Sape

DOI
10.1016/j.oceaneng.2022.111347

Publication date
2022

Document Version
Final published version

Published in
Ocean Engineering

Citation (APA)
Tan, J., Polinder, H., Laguna, A. J., & Miedema, S. (2022). A numerical study on the performance of the point absorber Wave Energy Converter integrated with an adjustable draft system. *Ocean Engineering*, *254*, Article 111347. https://doi.org/10.1016/j.oceaneng.2022.111347

Ocean Engineering 254 (2022) 111347

Contents lists available at ScienceDirect

Ocean Engineering

journal homepage: www.elsevier.com/locate/oceaneng

A numerical study on the performance of the point absorber Wave Energy Converter integrated with an adjustable draft system

Jian Tan *, Henk Polinder, Antonio Jarquin Laguna, Sape Miedema

Department of Maritime & Transport Technology, Delft University of Technology, The Netherlands

ARTICLE INFO

Keywords:
Wave Energy Converters
Adjustable draft system
Nonlinear time domain modeling

ABSTRACT

The Power Take-Off (PTO) rating of Wave Energy Converters (WECs) is generally much higher than the average extracted power. Scientific literature has indicated that downsizing the PTO capacity to a suitable level is beneficial for improving the techno-economic competitiveness. In this paper, a novel design, namely the adjustable draft system, is proposed for point absorbers to implement PTO downsizing. A frequency domain model is established to calculate the performance of the proposed device. From frequency domain analysis, two potential advantages are identified by installing the adjustable draft system. Firstly, the excitation force can be controlled by adjusting the buoy draft, which could be utilized to reduce the required PTO force. This is helpful for downsizing the PTO capacity. Secondly, the relevant natural frequency of the point absorber can be adapted to the operating wave states by varying the buoy draft, which improves the power absorption. A nonlinear approach is adopted specifically for the spherical buoy to include the nonlinear Froude–Krylov force and viscous drag force. The results show that the nonlinear forces have a significant influence on the power absorption when operating close to resonance regions. However, the advantages resulting from the proposed system still can be observed while considering the nonlinear forces. The power absorption can be improved by 27% and 12% in particular cases of regular and irregular wave states respectively.

1. Introduction

Ocean waves carry large amounts of clean energy, which can make a significant contribution to global energy demand. A number of technologies has been proposed to convert wave energy to usable electricity, but wave energy has not yet been widely utilized (Aderinto and Li, 2018; Lehmann et al., 2017). As one of the important barriers, the high Levelized Cost Of Energy (LCOE) makes WECs not as competitive as other renewable energy technologies (De Andres et al., 2017).

An important reason why the economic performance of WECs is not competitive is that the PTO capacity is generally oversized with regard to the average extracted power (Tai et al., 2012). In fact, the cost of PTO systems normally accounts for over 20% of the total Capital Expenditures (CAPEX), and oversized PTO systems are not economically favorable (Tan et al., 2022). The difficulty in downsizing the PTO capacity lies mainly on the characteristics of the wave resource. Typically, the input wave power in real sea conditions is highly fluctuating and the peak wave power is nearly ten times the average power during a given sea state (Prado and Polinder, 2013b). To capture more wave power, the rating of PTO systems is designed to be much higher than the average absorbed power (Prado and Polinder, 2013a). Besides, larger PTO capacities are beneficial for WECs sustaining the highly fluctuating wave power without damaging the device. For instance, enlarging the stroke and the size of the PTO system can be used to reduce the occurrence of the violation of the displacement and PTO force constraints (Backer, 2009; Sergiienko et al., 2018).

The impact of PTO sizing on the power performance of WECs has been investigated in scientific literature. The PTO size is commonly indicated by its force limit, rated power or peak power. The downsized PTO capacities are thus associated with tighter force or power constraints. One approach to comply with the downsized PTO systems is to take the corresponding constraints into account when tuning the PTO control parameters. For instance, a PTO sizing method was presented in Tan et al. (2021a), in which the parameters could be optimized to maximize the extracted power with the given force constraint. In Backer (2009), the hydrodynamic optimization of a point absorber was conducted, and the PTO parameters were tuned with the given force and displacement constraints. The results showed that the PTO force limit can not only affect the geometry optimization but also dramatically penalize the power absorption, especially at powerful wave states. Alternatively, PTO downsizing can be realized by changing the control strategy. In Tai et al. (2012), Shek et al. (2008), Tedeschi and Molinas (2010b, 2012), Tedeschi et al. (2011) and Wang et al.

* Corresponding author.
E-mail address: J.TAN-2@tudelft.nl (J. Tan).

https://doi.org/10.1016/j.oceaneng.2022.111347
Received 20 May 2021; Received in revised form 18 March 2022; Accepted 15 April 2022
Available online 5 May 2022

(2022, 2020), a series of studies focusing on the influence of the control strategy on PTO rating and power performance was conducted through numerical simulation and experiments. It was concluded that reactive control strategies could improve the average extracted power remarkably but result in a higher peak to average power ratio. Comparatively passive control strategies require a lower PTO force and peak power rating but correspond to a lower PTO average power absorption. The research reviewed indicates a conflicting requirement between maximizing the PTO power absorption and downsizing its capacity, where a compromise between these two aspects is required. Hence this paper proposes an alternative approach to downsize the PTO rating while retaining the power performance at an adequate level.

The adjustable draft system is investigated in this paper to implement the PTO downsizing of a heaving point absorber, in which the buoy draft can be ideally adjusted to vary the hydrodynamic properties of the WEC. The effect of the buoy draft on the performance of WECs has been investigated in literature (Wen et al., 2018; Shadman et al., 2018; Al Shami et al., 2019; Wang and Ringwood, 2021; Kurniawan and Moan, 2013; Stallard et al., 2009). Generally, the effect was discussed in studies focusing on geometry optimization of the WEC's floating buoy. In most cases, the buoy draft has been proven to be related to the energy absorption efficiency and the absorption bandwidth of WECs, although the specific effect differs with the buoy geometry and size (Wen et al., 2018; Shadman et al., 2018; Al Shami et al., 2019; Kurniawan and Moan, 2013; Wang and Ringwood, 2021). Besides, the influence of the buoy draft adjustment on the hydrodynamic performance of WECs was investigated in Stallard et al. (2009), which was intended to explore the possibility for limiting the heaving motion of WECs in extreme waves by the buoy draft adjustment with upper surface immersion. Their results showed that the increase of the buoy draft causes the increase of both the natural period and the hydrodynamic damping, and the buoy motion can be reduced efficiently by increasing the floater's mass. In Stallard et al. (2009), a valuable insight about the possibilities of making the hydrodynamic performance of WECs variable by the buoy draft adjustment was provided, which also inspired the work in this paper. However, the utilization of the buoy draft adjustment for downsizing the PTO capacity and improving the power performance has not been widely discussed. In previous work (Tan et al., 2020), the adjustable draft system for the use of PTO downsizing was introduced for the first time, but the focus was mainly on the preliminary conceptual design.

This paper aims at investigating the power performance of a point absorber integrated with an adjustable draft system by means of numerical simulation. For this purpose, this paper first provides an insight into the influence of the buoy draft adjustment on the hydrodynamic performance of a spherical heaving point absorber. Then, it reveals the contribution of the adjustable draft system to the adjustment of the required PTO force. Finally, this paper looks at the improvement resulting from integrating the adjustable draft system with a point absorber on the power performance.

An adjustable draft system is proposed for downsizing the PTO capacity. First, the point absorber concept and the adjustable draft system are described. Next, a frequency domain model is established to study the performance of the adjustable draft WEC. Based on the frequency domain analysis, the effects of the draft adjustment on PTO performance and natural frequencies of the buoy are discussed. The variation of the required PTO force and absorbed power with the buoy draft is presented. In addition, a comparison between power performance of the adjustable draft WEC and fixed draft WEC is made. Furthermore, to improve the accuracy, a time domain model is used to take into account the nonlinear forces. The impact of the nonlinear forces on the absorbed power of the adjustable draft WEC is shown. The improvement on the power performance resulting from the adjustable draft system is evaluated based on the nonlinear time domain model, and both regular and irregular wave states are considered.

2. Concept description

This section describes the concept of the adjustable draft WEC. A generic heaving point absorber is used as the WEC reference in this study. The geometry of the floating buoy is a sphere with a diameter of 5.0 m. The schematic of the adjustable draft WEC concept is shown in Fig. 1. In this concept, a ballast pump is installed inside the buoy for implementing the buoy draft adjustment. The minimal and the maximal adjusted buoy draft are defined as 0.50 and 0.75 times the buoy diameter respectively. In principle, it is possible to extend the adjustable draft to a wider range by this adjustable draft system. However, further increasing the buoy draft could result in the occurrence probability of the floating buoy's being fully submerged and breaching the water surface during the operation, which could bring in excessive losses due to surface tension. On the contrary, by means of the adjustable draft system, it is possible to decrease the draft to less than 0.5 times the diameter. But the lower buoy drafts improve the chances of the buoy leaving and then impacting on the water, causing slamming loads harmful to the structure (Backer, 2009). As a consequence, both these two phenomena should be avoided as much as possible in designing WECs. In addition, both the effects are coupled with highly nonlinear behaviors (Sergiienko et al., 2017), which are outside the scope of this study. Thus, the adjustable range of the buoy draft is defined between 2.50 m and 3.75 m in the present study and the adjustable range of the draft h_a is 1.25 m. This designed range could be varied according to the buoy geometry and size.

The total mass of the buoy can be changed by varying the ballast water inside the buoy. It is assumed that the buoy without ballast water naturally floats at the minimum draft of 2.50 m in still water. To reach each desired buoy draft, the ballast water inside the buoy is regulated by the pump to make the buoy float in equilibrium. It is realized that the ballast water inside the buoy could cause sloshing during the movement of the buoy. Sloshing affects the dynamics of the buoy, which might reduce the stability and controllability of the system. To avoid this issue, one possible solution is to install multiple ballast segments inside the buoy. To implement the buoy adjustment, each segment can only be fully loaded or drained out. In this way, sloshing inside the buoy can be expected to be mitigated.

The floating buoy is connected to the moving part of the PTO by a rod, and the moving part could be a piston or generator translator depending on the PTO type. However, as the PTO position is fixed, the variation of the buoy draft has an influence on the allowable stroke of the PTO. To avoid this issue, a hydraulic clamp is used. When the buoy draft varies, the clamp adjusts the rod length correspondingly and stores the additional part of the rod inside the buoy. In this way, the allowable PTO stroke remains identical when the buoy draft changes. It is realized that the control strategy and efficiency of the ballast pump and hydraulic clamp have in practice an influence on performance of the whole system, but it is assumed that the draft could always be adjusted to the expected value in each wave state. In addition, the displacement of the buoy is limited to protect the structure, and it is limited to 0.4 times the diameter of the buoy in this paper. Furthermore, a passive control strategy is implemented for the studied point absorber, which implies that only a force proportional to buoy velocity is applied by the PTO system.

3. Numerical modeling

This section is composed of two parts. Firstly, the equations of motion and frequency domain modeling of WECs are presented. Secondly, an algebraic nonlinear time domain model for considering the nonlinear Froude–Krylov force and the viscous drag force is introduced.

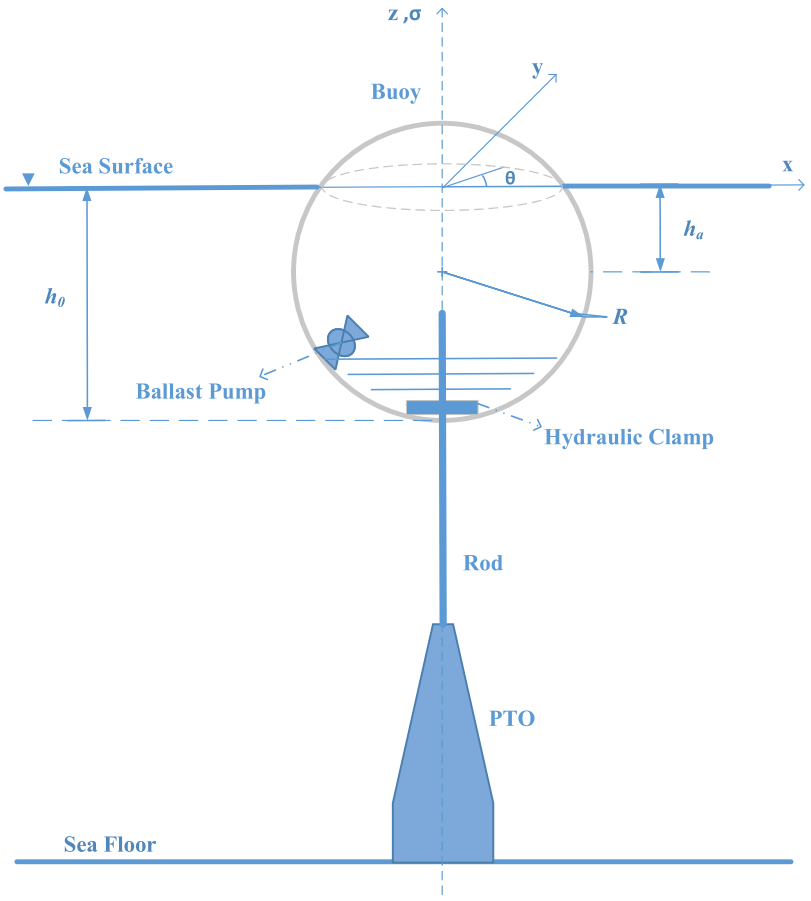

Fig. 1. Schematic of the spherical point absorber with the adjustable draft system. R, h_a and h_0 represent the buoy radius, the adjustable draft range and the buoy draft.

3.1. Frequency domain model

In this subsection, the frequency domain model of the studied WEC is presented based on linear wave theory. As the device in this paper is assumed to oscillate only in heave motion, the frequency domain model is only discussed for this degree of freedom. According to Newton's second law, the motion of the WEC as a rigid body can be described as

$$m\frac{\mathrm{d}\boldsymbol{u}(t)}{\mathrm{d}t} = \boldsymbol{F_{hs}}(t) + \boldsymbol{F_e}(t) + \boldsymbol{F_{pto}}(t) + \boldsymbol{F_r}(t) \tag{1}$$

where m is the mass of the oscillating body, $\boldsymbol{F_{hs}}$ is the hydrostatic force, $\boldsymbol{F_e}$ is the wave excitation force, $\boldsymbol{F_r}$ is the wave radiation force, $\boldsymbol{F_{pto}}$ is the PTO force and $\boldsymbol{u}$ is the velocity of the rigid body. If the body is assumed to undergo harmonic motion under regular waves and a linear PTO model is used to simulate the behavior of the PTO system, (1) could be rewritten in the form of complex amplitudes (Falnes, 2003), as

$$\hat{F}_e(\omega) = [R_i(\omega) + R_{pto}]\hat{u} + \mathrm{i}\omega\hat{u}[m + M_r(\omega)] + \mathrm{i}\hat{u}[-\frac{K_{pto}}{\omega} - \frac{S_{wl}}{\omega}] \tag{2}$$

where $R_i(\omega)$ is the hydrodynamic damping coefficient, R_{pto} is the PTO damping coefficient, ω is the wave frequency, $M_r(\omega)$ is the added mass of the buoy, $\hat{u}$ is complex amplitude of the vertical velocity, K_{pto} is the PTO stiffness coefficient and S_{wl} is the hydrostatic stiffness. The intrinsic impedance of the heaving buoy and PTO impedance can be introduced as

$$Z_i(\omega) = R_i(\omega) + \mathrm{i}X_i(\omega) \tag{3}$$

$$X_i(\omega) = \omega[m + M_r(\omega)] - \frac{S_{wl}}{\omega} \tag{4}$$

where $Z_i(\omega)$ is the intrinsic impedance of the heaving buoy and $X_i(\omega)$ is the intrinsic reactance. Similarly, the impedance of the PTO system is given as

$$Z_{pto}(\omega) = R_{pto}(\omega) + \mathrm{i}X_{pto}(\omega) \tag{5}$$

$$X_{pto}(\omega) = -\frac{K_{pto}}{\omega} \tag{6}$$

where $Z_{pto}(\omega)$ is the PTO impendence and $X_{pto}(\omega)$ is the PTO reactance. As a passive control strategy is considered for the PTO system, only PTO damping force is applied on the WEC, and (2) is rewritten as

$$\hat{F}_e(\omega) = [Z_i(\omega) + R_{pto}(\omega)]\hat{u} \tag{7}$$

The hydrodynamic characteristics of floating bodies, including $M_r(\omega)$, $R_i(\omega)$ and $F_e(\omega)$, are calculated numerically using the Boundary Element Method through the open source software Nemoh (Babarit and Delhommeau, 2015). The accuracy of Nemoh has been validated for WEC applications in Penalba et al. (2017), Guo et al. (2017) with experimental results and by comparison with other numerical packages. Then, by solving (7), the complex amplitude of velocity $\hat{u}$ could be obtained as

$$\hat{u} = \frac{\hat{F}_e}{Z_i + R_{pto}} \tag{8}$$

In regular wave conditions, the time averaged absorbed power can be obtained and expressed as

$$\overline{P} = \frac{1}{2}R_{pto}\,|\hat{u}|^2 \tag{9}$$

The complex amplitude of PTO force could be expressed as:

$$\hat{F}_{pto} = R_{pto}\hat{u} \tag{10}$$

Substituting (8) to (10) gives the amplitude of PTO force:

$$\left|\hat{F}_{pto}(\omega)\right| = \left|R_{pto}\frac{\hat{F}_e(\omega)}{Z_i + R_{pto}}\right| = \frac{\left|R_{pto}\right|}{\left|Z_i + R_{pto}\right|}\left|\hat{F}_e(\omega)\right| \tag{11}$$

The determination of the PTO damping coefficients R_{pto} is influential to the dynamic response and power absorption of WECs. In Tan et al. (2021a), a theoretical method was derived based on the frequency domain model to calculate the optimal PTO damping coefficients for maximizing the power absorption in regular wave conditions. The physical constraints can be considered in the tuning of PTO parameters, by which the harmonic amplitudes of the PTO force and buoy displacement are limited within the given range. Specifically, with the passive control strategy, the displacement limit is associated with the minimal allowed PTO damping while the PTO force limit implies the maximum allowed PTO damping (Tan et al., 2021a). Here, the theoretical method is adopted to optimize the PTO damping coefficient for each wave state.

It must be acknowledged that the frequency domain modeling has limited applicability as it is restricted to linear assumptions. The accuracy of the frequency domain modeling around the resonance of WECs is limited where the displacement is too high and the linear assumptions are violated (Penalba et al., 2017a). However, the amplitude of the harmonic displacement of the buoy does not exceed 0.4 times the diameter in this concept, which eases the violation (Sergiienko et al., 2017). In addition, the computational efficiency of frequency domain modeling is much higher than other approaches, which makes it suitable for identifying the power performance of WECs in early design stages.

3.2. Nonlinear time domain model

Scientific literature (Giorgi and Ringwood, 2017b,c) has indicated that the non-uniform buoy cross-sectional area could make the effect of the nonlinear Froude–Krylov force pronounced. In addition, the draft adjustment of the buoy is expected to affect the significance of the nonlinear Froude–Krylov force. Therefore, it is necessary to investigate the influence of the nonlinear Froude–Krylov forces on the performance of the studied WEC. In Giorgi and Ringwood (2017b) and Giorgi et al. (2021), a computationally efficient nonlinear model was proposed for axisymmetric and prismatic geometries, and the model uses an algebraic solution to the Froude–Krylov force integral. The proposed nonlinear Froude–Krylov model is adopted in the present paper for the adjustable draft WEC. Regarding more complex geometries, numerical approaches can be applied to compute the nonlinear Froude–Krylov force (Penalba Retes et al., 2015). For example, in the open-source software WEC-Sim, the nonlinear Froude–Krylov force is calculated by integrating the pressure over each pre-meshed panel of the instantaneous wetted surface (Lawson et al., 2014a). However, compared with the analytical model, the numerical routines are inevitably associated with higher computational times. The formulation of the analytical nonlinear Froude–Krylov model is briefly presented in the following text, and more details can be found in Giorgi and Ringwood (2017b).

In the model, the incoming waves are represented based on the linear wave theory, and all the considered waves are assumed to be unidirectional. The responses of the WEC in both regular and irregular wave conditions are investigated. The regular wave input is described as harmonic waves which can be expressed as

$$\eta(t) = \zeta_a \cos(\lambda x - \omega t) \tag{12}$$

where t is time, λ is the wave number, ω is the angular frequency of the incoming wave and ζ_a is the wave amplitude. Given the linear wave theory, irregular waves can be represented by the superposition of a set of regular wave components, as

$$\eta(t) = \sum_{j=1}^{N} \zeta_a(\omega_j)\cos(\lambda(\omega_j)x - \omega_j t + \varphi(\omega_j)) \tag{13}$$

where $\lambda(\omega_j)$, $\zeta_a(\omega_j)$ and $\varphi_{(\omega_j)}$ are the wave number, wave amplitude and phase of the regular wave component corresponding to the frequency component ω_j. Regarding irregular wave conditions, the JONSWAP spectrum together with peakedness factor of 3.3 is applied (Cahill and Lewis, 2014). For each wave state, 500 individual harmonic wave components with a random set of phases between frequency components are considered. The angular frequencies of the wave components are uniformly spaced from 0.1 to 4.0 rad/s.

The Froude–Krylov force can be divided into static and dynamic terms. The static Froude–Krylov force is equivalent to the hydrostatic force in (1), and calculated by the balance between the gravity force and the buoyancy force:

$$\boldsymbol{F}_{\boldsymbol{FK}_{st}} = m\boldsymbol{g} - \iint_{S(t)} P_{st}\mathbf{n}\,\mathrm{d}S \tag{14}$$

where $\boldsymbol{F}_{\boldsymbol{FK}_{st}}$, $\boldsymbol{g}$, $S(t)$, P_{st} and $\boldsymbol{n}$ represent the static Froude–Krylov force, gravity acceleration, submerged surface, hydrostatic pressure and normal vector to the geometry surface. The dynamic Froude–Krylov force is expressed as:

$$\boldsymbol{F}_{\boldsymbol{FK}_{dy}} = -\iint_{S(t)} P_{dy}\mathbf{n}\,\mathrm{d}S \tag{15}$$

where here $\boldsymbol{F}_{\boldsymbol{FK}_{dy}}$ and P_{dy} represent the dynamic Froude–Krylov force and the dynamic pressure. The excitation force in (1) is calculated by the sum of the dynamic Froude–Krylov force and the diffraction force. Besides, the viscous drag force is also considered in the nonlinear time domain model. Therefore, (1) can also be expressed as

$$m\frac{\mathrm{d}\boldsymbol{u}(t)}{\mathrm{d}t} = \boldsymbol{F}_{\boldsymbol{FK}_{st}} + \boldsymbol{F}_{\boldsymbol{FK}_{dy}} + \boldsymbol{F}_{\boldsymbol{D}} + \boldsymbol{F}_{\boldsymbol{r}} + \boldsymbol{F}_{\boldsymbol{pto}} + \boldsymbol{F}_{\boldsymbol{vis}} \tag{16}$$

where $\boldsymbol{F}_{\boldsymbol{D}}$ is the diffraction force.

According to Falnes (2003), in deep water condition, the pressure resulting from the regular wave can be obtained based on Airy wave theory as

$$P(x,z,t) = \rho g\zeta_a e^{\lambda z}\cos(\omega t - \lambda x) - \rho g z \tag{17}$$

where x is the direction of wave propagation. For axisymmetric geometries, parametric cylindrical coordinates can be used to describe the geometry surface:

$$\begin{cases} x(\sigma,\theta) & = f(\sigma)\cos(\theta) \\ y(\sigma,\theta) & = f(\sigma)\sin(\theta),\ \theta \in [0,2\pi) \wedge \sigma \in [\sigma_1,\sigma_2] \\ z(\sigma,\theta) & = \sigma \end{cases} \tag{18}$$

where $f(\sigma)$ is the function describing the geometry profile. For the heaving point absorber, only the force in the vertical direction is considered. In regular waves, the magnitude of the total Froude–Krylov force in vertical direction can be expressed as

$$\begin{aligned} \boldsymbol{F}_{\boldsymbol{FK}_z} &= \int_0^{2\pi}\int_{\sigma_1}^{\sigma_2} P(x(\sigma,\theta), z(\sigma,\theta), t) f'(\sigma) f(\sigma)\mathrm{d}\sigma\mathrm{d}\theta \\ &= \int_0^{2\pi}\int_{\sigma_1}^{\sigma_2} (\rho g\zeta_a e^{\lambda\sigma}\cos(\omega t - \lambda f(\sigma)\cos(\theta)) - \rho g\sigma)\cdot f'(\sigma) f(\sigma)\mathrm{d}\sigma\mathrm{d}\theta \end{aligned} \tag{19}$$

The integral limits of the wetted surface is defined as

$$\begin{cases} \sigma_1 & = Z_d(t) - h_0 \\ \sigma_2 & = \eta(t) \end{cases} \tag{20}$$

where η is the elevation of the free surface at $x = 0$, Z_d is the vertical displacement of the buoy and h_0 is the draft of the buoy. The dependence of the pressure on x in (17) can be neglected in the long wave approximation which assumes that the wave length is much longer than the characteristic dimension of the buoy. Then the term $\cos\theta$ in (19) can be neglected correspondingly. The integral calculation of (19) for the heaving point absorber with centroid at the still water level has been explicitly derived in Giorgi and Ringwood (2017b). In

regular waves, the static and dynamic Froude–Krylov force for the spherical geometry with a given draft can be calculated as

$$\boldsymbol{F}_{\boldsymbol{FK}_{st}} = \int_0^{2\pi}\int_{\sigma_1}^{\sigma_2} P_{st_z}\mathrm{d}\sigma\mathrm{d}\theta = -2\pi\rho g\left[\frac{\sigma^3}{3} + (Z_d(t) - h_0 + R)\frac{\sigma^2}{2}\right]_{\sigma_1}^{\sigma_2} \quad (21)$$

$$\begin{aligned}\boldsymbol{F}_{\boldsymbol{FK}_{dy(re)}} &= \int_0^{2\pi}\int_{\sigma_1}^{\sigma_2} P_{dy_z}\mathrm{d}\sigma\mathrm{d}\theta \\ &= -\frac{2\pi}{\lambda}\rho g\zeta_a(\cos\omega t)\left[((Z_d(t) - h_0 + R) + \frac{1}{\lambda} - \sigma)e^{\lambda\sigma}\right]_{\sigma_1}^{\sigma_2}\end{aligned} \quad (22)$$

where R is the radius of the buoy. The superposition theory can be applied to calculate the dynamic Froude–Krylov force in irregular waves, while it is noted that (21) is also applicable for the calculation of the static Froude–Krylov force in irregular waves. In addition, the formulation for computing other forces remain same in irregular waves. According to (13) and (22), the dynamic Froude–Krylov force in irregular waves can be expressed as

$$\begin{aligned}\boldsymbol{F}_{\boldsymbol{FK}_{dy(irr)}} = \sum_{j=1}^{N} &-\frac{2\pi}{\lambda(\omega_j)}\rho g\zeta_a(\omega_j)(\cos(-\omega_j t + \varphi(\omega_j))) \\ &\left[((Z_d(t) - h_0 + R) + \frac{1}{\lambda(\omega_j)} - \sigma)e^{\lambda(\omega_j)\sigma}\right]_{\sigma_1}^{\sigma_2}\end{aligned} \quad (23)$$

According to Cummins equation (Cummins et al., 1962), the radiation force is calculated as

$$\boldsymbol{F}_{\boldsymbol{r}}(t) = -\int_{-\infty}^{t} K_{rad}(t-\tau)u(\tau)\mathrm{d}\tau - M_r(\infty)a(t)\mathrm{d}t \quad (24)$$

where $M_r(\infty)$ is the added mass evaluated at the infinite frequency, K_{rad} is the radiation impulse function, and they can be calculated based on the results $R_i(\omega)$ and $M_r(\omega)$ obtained from Nemoh. To compute the convolution integral efficiently, the state-space approximation is used (Pérez and Fossen, 2008). According to Giorgi and Ringwood (2017b), the diffraction force is calculated as

$$\boldsymbol{F}_{\boldsymbol{D}}(t) = -\int_{-\infty}^{\infty} K_{diff}(t-\tau)\eta(\tau)\mathrm{d}\tau \quad (25)$$

where K_{diff} is the diffraction impulse function.

In the nonlinear time domain simulation, an end-stop mechanism is applied to limit the excessive displacement. The end stop force is expressed as

$$\boldsymbol{F}_{\boldsymbol{es}}(t) = \begin{cases} 0, & |Z_d(t)| \le S_m \\ -K_{es}\frac{Z_d(t)-S_m}{|Z_d(t)-S_m|}|Z_d(t) - S_m|, & |Z_d(t)| > S_m \end{cases} \quad (26)$$

where K_{es} is the stiffness coefficient of the end stop spring, and it is set as 500 kN/m in this work.

The viscous drag force is represented by a quadratic damping term which is similar to the drag component in Morison's equation (Babarit et al., 2012), as

$$\boldsymbol{F}_{\boldsymbol{vis}} = -\frac{1}{2}\rho C_D A_D|\boldsymbol{u} - \boldsymbol{u_0}|(\boldsymbol{u} - \boldsymbol{u_0}) \quad (27)$$

where ρ is the water density, C_D is the drag coefficient, A_D is the characteristic area of the buoy, and $\boldsymbol{u_0}$ is the undisturbed flow velocity at the centroid of the buoy. The drag coefficient is selected as 0.6 to minimize the error of the power estimate based on the investigation reported in Giorgi and Ringwood (2017a), in which the research reference is also a sphere.

During the calculation of the nonlinear Froude–Krylov force, the static and dynamic pressures are integrated over the wetted surface of the buoy. The pressure is obtained based on linear wave theory, and the pressure field is described by (17). It is clear that the values of the pressure would be overestimated when the surface area of interest moving above the mean free surface, since z is in the exponential term in (17). To enhance the accuracy of the model, Wheeler stretching theory is used to correct the pressure expression. In this sense, the flow velocity and pressure at the initial vertical position z is replaced by those in a corrected vertical position z', and it can be expressed as

$$z' = \frac{D(D+z)}{D+\eta} - D \quad (28)$$

where D is the water depth. D is set as a sufficiently large value of 1000 in the numerical set-up, considering the deep water assumption in this work.

As nonlinear forces are taken into account, the optimal PTO damping coefficients could not be obtained theoretically. Thus, in the nonlinear time domain analysis, the PTO damping coefficients are selected through an exhaustively search approach. Specifically, the PTO damping is searched over the range $[0.01|Z_i(\omega)|, 2|Z_i(\omega)|]$ for regular waves or $[0.01|Z_i(\omega_p)|, 2|Z_i(\omega_p)|]$ for irregular waves, in which ω_p stands for the peak period of the irregular waves. The range was defined on the basis of linear hydrodynamics, $|Z_i(\omega)|$ has been proven to be the optimal damping for an unconstrained heaving point absorber with the passive control strategy in regular waves (Hals et al., 2002). In this paper, 200 evenly spaced values are considered in the range, and the PTO damping is selected to maximize the power absorption while complying with the PTO force limits.

The time domain simulation is performed based on the numerical integration scheme. The initial displacement and velocity of the buoy is set to zero. The simulation time duration and time step is set to 125 and 0.01 times the considered wave period (or peak period) respectively. A ramp function is used to avoid strong transient flow at earlier time steps, and the ramp time is chosen as 25 times the wave period (Lawson et al., 2014b). The duration of the ramp time is not included in the calculation of average power absorption. To mitigate random errors in the simulation with irregular waves, the time domain model is re-run ten times to calculate the mean value in each case.

4. Results and discussion

4.1. Frequency domain analysis

4.1.1. The influence of the buoy draft on the hydrodynamic performance

Based on frequency domain modeling, the effect of the draft adjustment on the hydrodynamic performance of the floating spherical buoy is investigated. First, the hydrodynamic coefficients of the spherical floating buoy in heave motion are calculated for different buoy drafts. The corresponding excitation force coefficients, added mass and radiation damping are depicted in Appendix B. Then, in the case without the PTO force applied on the buoy, the heave response amplitude operators (RAO) of the spherical floating buoy in different drafts are shown in Fig. 2. It can be noted that the heave RAO is highly dependent on the buoy draft. An increase of the buoy draft leads to a larger peak value of the heave RAO.

Fig. 3 presents the relative power absorption of the WEC with different buoy drafts, in which the PTO damping is tuned to maximize the absorbed power at the wave period of 5.0 s. The power absorption bandwidth is defined as a frequency range within which the WEC could absorb power higher than 50% of the maximum absorbed power. This measure effectively indicates the ability of the WEC responding to the incoming waves of frequencies rather than its natural frequency. Fig. 3 suggests that increasing the buoy draft reduces the power absorption bandwidth and a buoy with very large drafts could result in a narrow-banded device. However, the real sea conditions are normally characterized by irregular waves, in which a range of wave frequencies is included. As a result, a compromise is needed between pursuing a higher RAO in the peak period and a wider bandwidth when adjusting the buoy draft in irregular waves.

The total mass, water plane area, natural frequency and natural period of the WEC with different buoy drafts are shown in Figs. 4 and 5. It can be seen that the buoy draft adjustment makes a difference to these properties. The water-plane area and the natural frequency decrease with the increase of the buoy draft, but the total mass increases with the buoy draft.

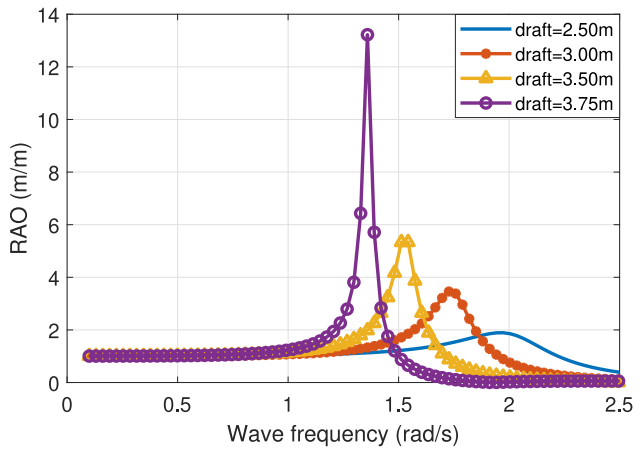

Fig. 2. Heave RAO of the floating spherical buoy of 5.0 m diameter in different drafts without PTO force.

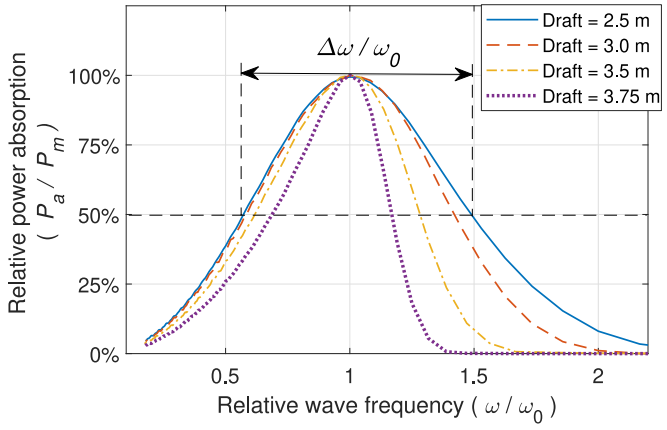

Fig. 3. The relative power absorption of the WEC with different buoy drafts. The results are calculated in regular wave states with a wave height of 1.0 m. P_a and P_m represent the absorbed power and the maximum absorbed power along various wave frequencies. ω_0 represents the wave frequency corresponding to the maximum power absorption.

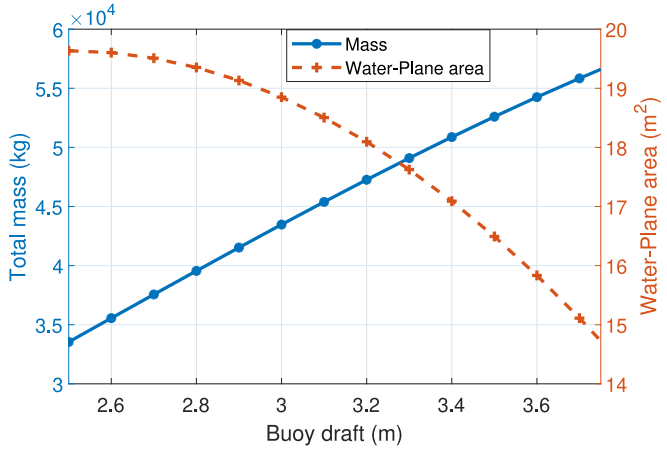

Fig. 4. The water plane area and total mass of the buoy as a function of the draft.

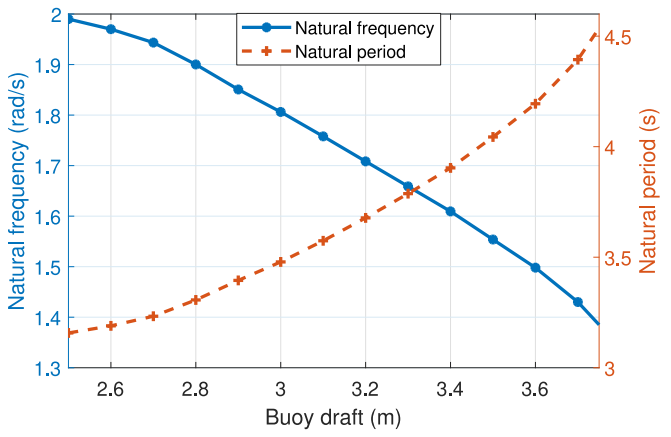

Fig. 5. The natural frequency and corresponding period of the heaving buoy as a function of the draft.

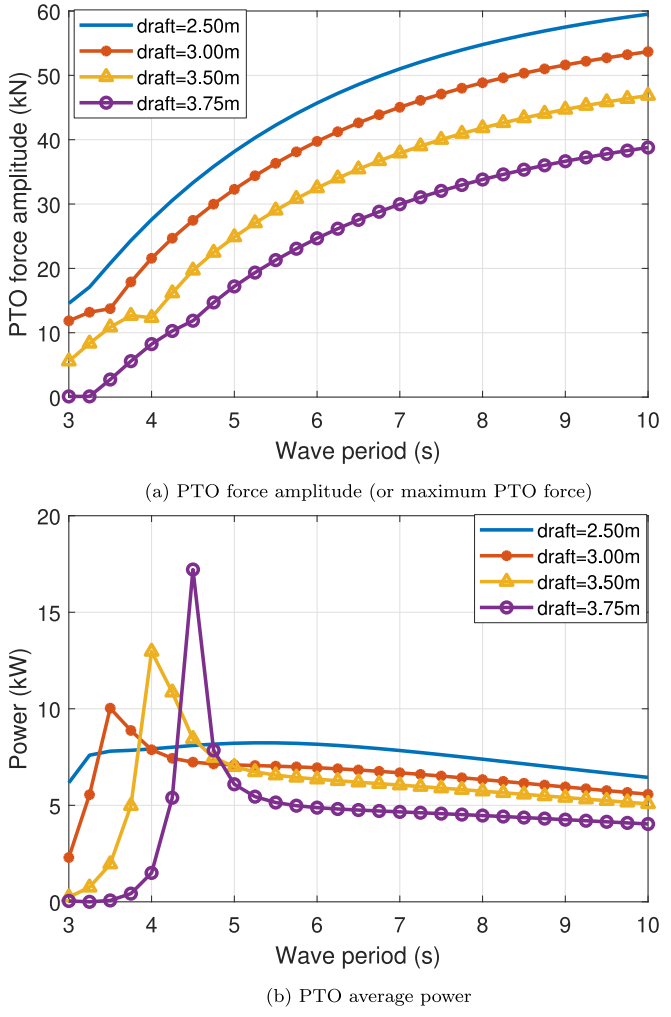

Fig. 6. PTO performance as a function of the buoy draft without force constraints, and the considered wave height is 1.0 m.

4.1.2. The influence of the buoy draft on the PTO performance

In this part, the effect of the buoy draft on the PTO performance is discussed. The PTO force amplitude and average absorbed power are calculated. It can be seen from Fig. 6 that the buoy draft significantly affects the PTO performance. Fig. 6(a) shows that the required PTO force amplitude can be reduced by increasing the buoy draft. As shown in Fig. 6(b), the impact of the draft adjustment on the average power is dependent on the wave period. The buoy drafts of 3.0 m and 3.5 m and 3.75 m correspond to natural periods of 3.5 s, 4.1 s and 4.5 s respectively. Thus, their average power are higher than that of the buoy

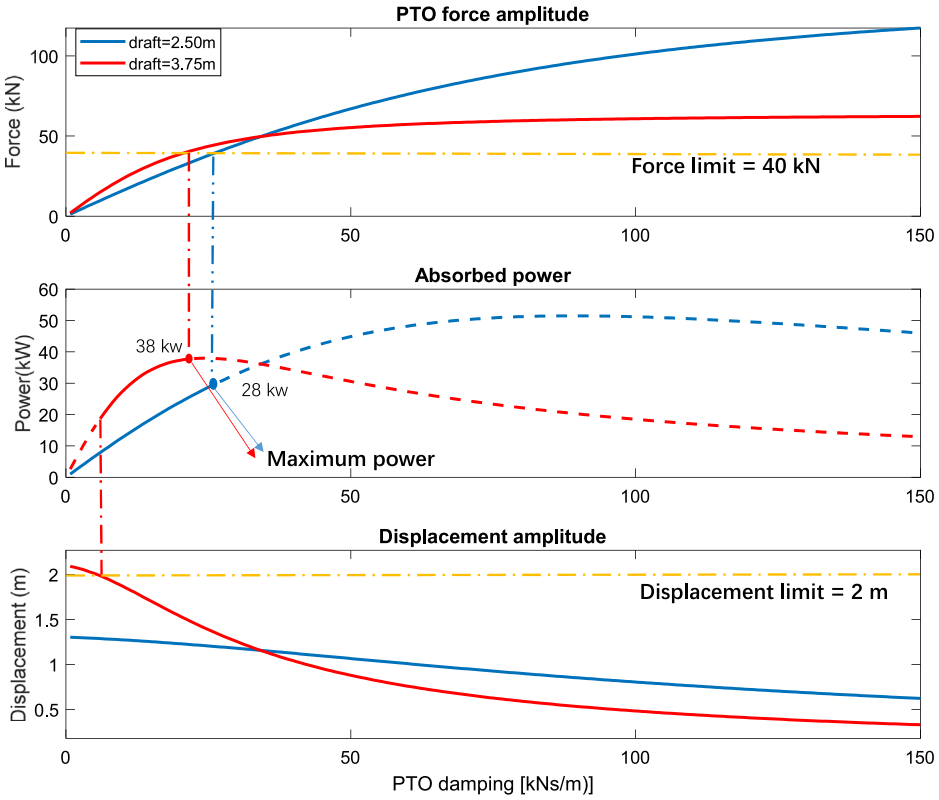

Fig. 7. The PTO force amplitude, average power and displacement as a function of PTO damping for two different buoy drafts. The considered wave height is 2.5 m and the wave period is 5.0 s.

draft of 2.5 m around the range of their natural wave periods. When the wave period is higher than 5.0 s, the buoy draft of 2.5 m is associated with a higher average power than that of other larger buoy drafts. It can be deduced that the buoy draft adjustment can be used to regulate the required PTO force. Therefore, adjusting the buoy draft is expected to enable downsizing of the PTO capacity. In addition, adapting the buoy draft to wave periods is able to improve the average power, because the natural frequency of the WEC can be controlled to match the wave period. For instance, the average power of the WEC with a buoy draft of 2.5 m is higher than that of other buoy drafts over a wide range of wave periods. However, it becomes lower than the average power of the WEC with larger buoy drafts along the wave period from 3.5 s to 4.8 s which matches the natural periods of larger buoy drafts as seen in Fig. 5.

4.1.3. Power performance with PTO force limits

As is shown before, the required PTO force of the WEC is related to the buoy draft. Thus, the effect of the PTO force constraints on power performance differs with the buoy draft. A good example is shown in Fig. 7, which presents the relationship between the PTO force, the average power and the PTO damping coefficient. The calculation is performed based on a regular wave state, in which the wave height and wave period are 2.5 m and 5.0 s respectively. It can be noted that a buoy draft of 2.5 m corresponds to a higher average extracted power than a buoy draft of 3.75 m without PTO force constraints. However, the implementation of the PTO force constraint would limit the available range of PTO damping coefficients, and the solid curves in the middle plot of Fig. 7 correspond to the available range of PTO damping coefficients. In this way, the absorbed power of the buoy draft of 3.75 m overtakes that with the buoy draft of 2.50 m, and they are 38 kW and 28 kW respectively with the PTO force limit of 40 kN. Therefore, it can be deduced that reasonably adjusting the buoy draft could mitigate the negative effect of PTO force limits on the power absorption.

To identify the influence of PTO force limits on the power performance of the WEC with different buoy drafts, various PTO force limits are implemented. The root mean square (RMS) value is commonly used in PTO rating, since it allows the PTO system, such as an electrical machine, to work in a sustainable condition on a longer time scale (Tedeschi and Molinas, 2010a). Thus, the PTO force limit is considered in the form of RMS value. Taking the wave state with a wave height of 1.0 m and wave period of 5.0 s as an example, the percentage of the absorbed power with force constrains to that without force constraints and the absorbed power per RMS of the required PTO force are presented in Fig. 8. It can be seen from Fig. 8(a) that PTO force limits have a notable negative influence on the power absorption. The percentage value increases with the PTO force limit. Besides, it can be seen that the percentage values of the WEC with the larger buoy drafts are generally higher than those with lower buoy drafts. This is expected since the WEC with the larger buoy drafts correspond to the lower required PTO forces at the unconstrained force condition, which has been shown in Fig. 6. In Fig. 8(b), it is seen that the absorbed power per RMS of the required PTO force tends to decrease with the force limit until the force limit is sufficiently high for the power absorption. It can also be noticed that the absorbed power per RMS of the PTO force differs with the buoy draft, and the buoy drafts of 3.75 m and 3.5 m are associated with higher values than that of the buoy draft of 2.5 m.

The power performance with force constraints is calculated for different wave periods, which is shown in Fig. 9. It can be noted that the increasing the buoy draft contributes to higher power absorption at low wave periods. With the increase of the wave period, the difference between the power performance of different buoy drafts tends to vanish. It should be realized that the power performance discussed in this paper is the absorbed power by the WEC instead of the grid power. This implies that the PTO efficiency is not taken into consideration. However, the force limit in reality represents the PTO size which

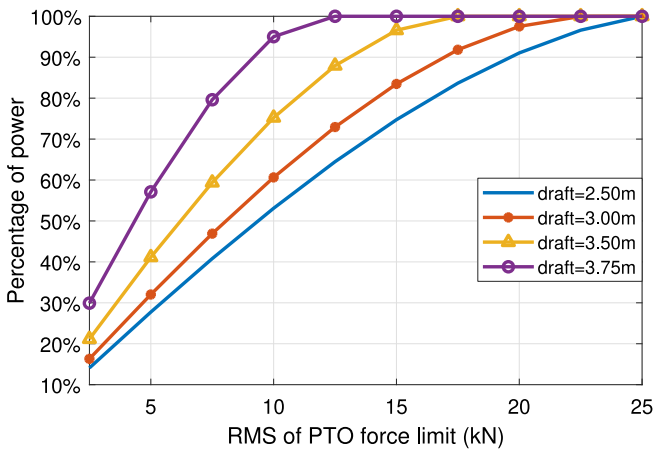

(a) Percentage of PTO absorbed power with force limits to that without force limits

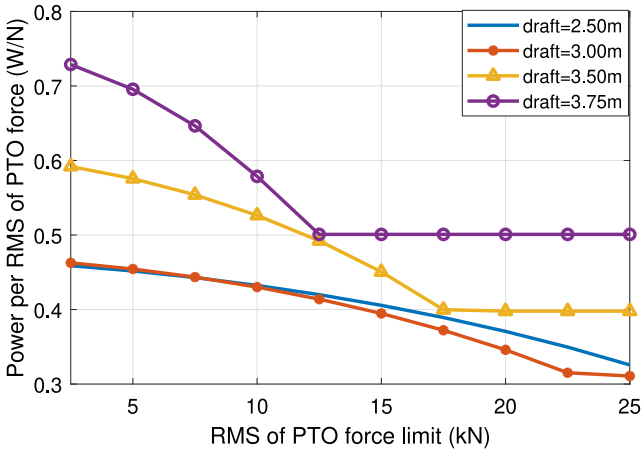

(b) PTO absorbed power per RMS of the PTO force

Fig. 8. The influence of PTO force limits on the power performance. The results are calculated in a regular wave state with the wave height of 1.0 m and the wave period of 5.0 s.

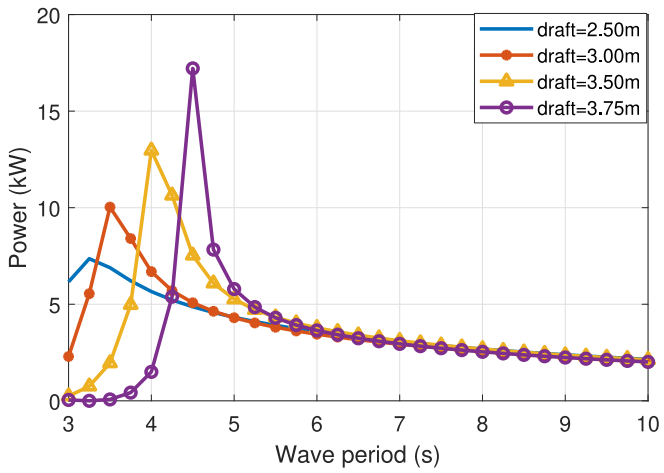

Fig. 9. The influence of PTO force limits on the power performance, with a wave height of 1.0 m and the RMS of the PTO force limit of 10 kN.

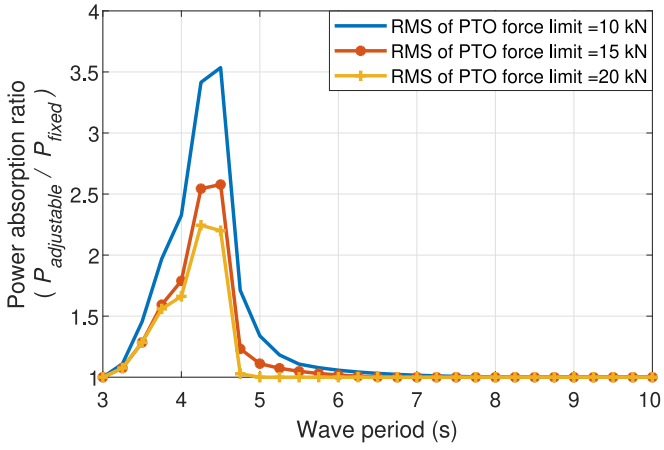

Fig. 10. Ratio of the power absorbed by the adjustable draft WEC to that by the fixed draft WEC in different RMS of the PTO force limit. The results are calculated in regular waves with a wave height of 1.0 m. $P_{adjustable}$ and P_{fixed} embody the power absorbed by the adjustable draft WEC and the power absorbed by the WEC with a fixed draft of 2.5 m.

could make a difference with respect to the PTO efficiency (Tokat and Thiringer, 2018). For instance, the relation of the PTO conversion efficiency to the size of linear generators in wave energy conversion has been investigated in Tan et al. (2021b). This study indicated that the overall power conversion efficiency generally increases with the dimension of linear generators, which mainly results from the reduction of copper losses in power conversion.

4.1.4. Performance comparison between the adjustable draft WEC and the fixed draft WEC

To present the benefits of the adjustable draft system, a comparison is made between the power absorption of the adjustable draft WEC and the fixed draft WEC. In this paper, fourteen buoy drafts evenly spaced along the adjustable range are considered when identifying the performance of the adjustable draft WEC. However, it should be realized that a continuous adjustment can be achieved in practice by the adjustable draft system. Regarding the fixed draft WEC, the buoy draft is fixed at 2.5 m. The ratios of power absorbed by the adjustable draft WEC to that by the fixed draft WEC are calculated, and the results are shown in Fig. 10. In the calculation, three different PTO force limits are implemented, and regular wave states with a wave height of 1.0 m are considered. It can be observed from Fig. 10 that the adjustable draft WEC is clearly associated with an improvement of the power absorption, compared with the fixed draft WEC. For instance, at the RMS of the PTO force limit being 10 kN, the absorbed power of the adjustable draft WEC is 3.5 times that of the fixed draft WEC. The improvement occurs over a wider range of wave periods with the stricter PTO force constraints. With the RMS of the PTO force limit of 10 kN, the improvement can be noticed from the wave period of 3.5 s until 6.5 s. However, it is observed only until around 4.8 s when the RMS of the PTO force limit increases to 20 kN. Therefore, it is concluded that the adjustable draft system is beneficial for the power absorption, especially with the downsized PTO capacity. It has to be acknowledged that the improvement of power absorption concentrates on the low wave periods (from 3.0 to 6.5 s). Thus, given the considered buoy size and geometry, its contribution for realistic wave sites where long wave periods are significantly dominating is relatively limited.

4.1.5. The influence of buoy size on the performance of the adjustable draft system

The effect of the draft adjustment on the hydrodynamics and PTO performance of the system depends on the buoy geometry and size. Here, the influence of the buoy size on the performance of the adjustable draft WEC is demonstrated. Froude scaling law is used to scale the buoy geometry (Payne, 2008), in which the hydrodynamic

Table 1
Froude scaling law for various quantities.

$k = \frac{L_s}{L_o} = \frac{H_s}{H_o}$
$\omega_s = \omega_o k^{-0.5}$
$T_s = T_o k^{0.5}$
$F_s = F_o k^3$
$B_{r\_s} = B_{r\_o} k^{2.5}$
$M_{r\_s} = M_{r\_o} k^3$
$h_{a\_s} = h_{a\_o} k$

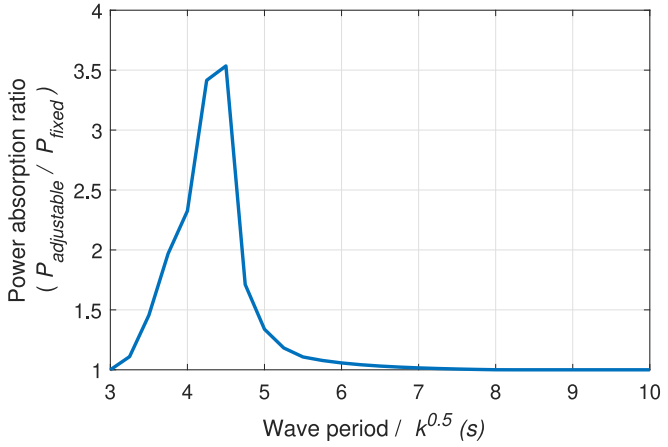

Fig. 11. Ratio of the power absorbed by the adjustable draft WEC to that by the fixed draft WEC for different buoy sizes, the wave heights and the RMS of the PTO force limit are $1.0 \cdot k$ m and $10 \cdot k^3$ kN. $P_{adjustable}$ and P_{fixed} embody the power absorbed by the adjustable draft WEC and the power absorbed by the WEC with a fixed draft of $2.5 \cdot k$ m.

coefficients, geometrical and wave parameters are obtained following Table 1. In the Table, k is the scale factor of the buoy; L is the geometrical length of the buoy; ω, T and H are the wave frequency, wave period and the wave height; F, B_r and M_r embody the force, the radiation damping and the added mass coefficients respectively; the subscript s and o represent the "scaled device" and the "original device" respectively.

Fig. 11 depicts how the buoy scaling affects the ratio between the power absorption of the adjustable draft WEC and the fixed draft WEC. It can be seen that the profile of the ratio does not change with the scaling factor, but the wave period changes accordingly. With the increase of the buoy size, the improvement of the power absorption moves to larger wave periods. Therefore, buoy scaling can be used to adapt the adjustable draft WEC to different wave climates.

4.2. Nonlinear time domain analysis

4.2.1. The effect of nonlinear forces on power performance

For simplification, only the buoy with a diameter of 5.0 m is discussed in the nonlinear time domain analysis, although the buoy size has been proven influential in Section 4.1.5. To verify the reproduced nonlinear time domain model, a comparison is made between the results of RAOs from the reproduced model and the results from Giorgi and Ringwood (2017b), which can be found in Appendix C. To identify the influence of the nonlinear forces on power performance of WECs, the results of the power absorption estimated by the nonlinear time domain model and linear model are compared, as shown in Fig. 12. The considered wave height is 1.0 m, and the RMS of the PTO force limit is 10 kN. The selection of the PTO damping is different for each model, thus the influence of the numerical model response on the optimization of the PTO damping is also reflected in the figure. It can be seen

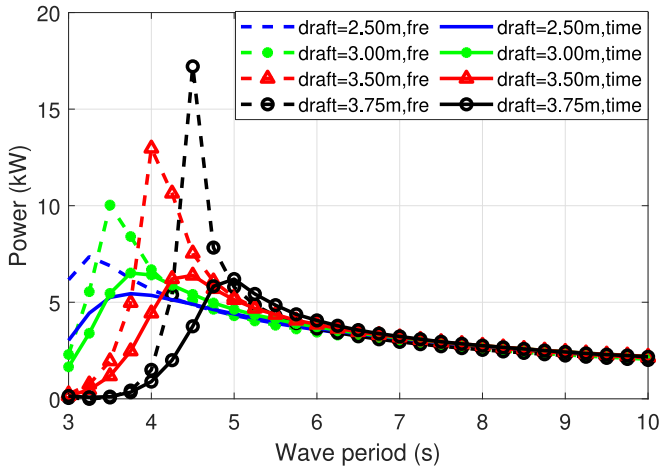

Fig. 12. Average power calculated by the nonlinear time domain model and frequency domain model for different buoy drafts. The results are calculated in regular wave states with a wave height of 1.0 m and the RMS of the PTO force limit is 10 kN. In the legend, "fre" and "time" represent the frequency domain model and nonlinear time domain model respectively.

from Fig. 12 that the power estimated by the nonlinear time domain model is much lower than that by the frequency domain model around the resonance regions, but the difference is negligible at other wave periods. For instance, the buoy draft of 3.75 m is associated with 17 kW at the wave period of 4.5 s in the frequency domain analysis, while it decreases to around 4 kW in the nonlinear time domain analysis. Therefore, the linear model overestimates the power performance around the resonance. The variation of the instantaneous wetted surface is expected to be the main contributor to the difference between the linear and nonlinear models. To reflect the variation, the standard deviations of the instantaneous displacement of the buoy relative to the wave elevation and the standard deviation of the instantaneous variation of the water-plane area are calculated for different buoy drafts, shown in Figs. 13 and 14. It is visible that the standard deviation of the relative displacement is clearly higher in the wave periods of resonance for each buoy draft. In addition, it is observed from Fig. 12 that the difference of power estimation between these models turns out to be larger for larger buoy drafts. This is expected since larger buoy drafts essentially correspond to larger variations of the water-plane area, as shown in Fig. 14. The variation of the water-plane area effectively implies the nonlinearity of the Froude–Krylov force.

Furthermore, as a consequence of the addition of nonlinear force components, the natural frequency is shifted to be lower. As can be seen in Fig. 12, the wave periods when maximum power is obtained deviate from those presented by the frequency domain analysis. Taking the buoy draft of 3.75 m as an example, the maximum power is obtained at 4.5 s in the frequency domain modeling, while it is at around 5.0 s in the nonlinear time domain analysis.

4.2.2. The influence of PTO force limits on power performance

The power performance of the WEC with different buoy drafts is calculated by the nonlinear time domain model, and various PTO force limits are implemented. The results are shown in Fig. 15, and the considered wave height and period are 1.0 m and 5.0 s respectively. It can be noted from Fig. 15(a) that the PTO force limit reduces the power absorption, but the effect differs with the buoy draft. For example, at the RMS of the PTO force limit of 10 kN, the percentage of the buoy draft of 3.75 m reaches nearly 100% while it is only around 55% for the buoy draft of 2.50 m. This observation generally agrees with the results obtained by the frequency domain analysis. Besides, comparing Fig. 15(b) and Fig. 8(b), it is seen that both their profiles suggest the similar trend, in which the power per RMS of the PTO force generally

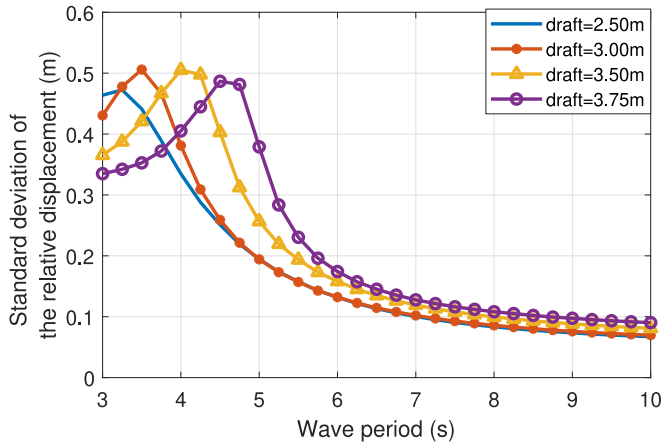

Fig. 13. The standard deviation of the displacement of the buoy relative to the wave elevation. The results are calculated in regular wave states with a wave height of 1.0 m, and the RMS of the PTO force limit is 10 kN.

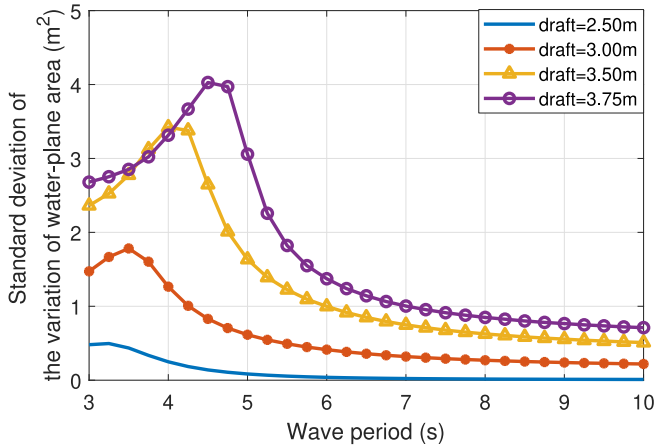

Fig. 14. The standard deviation of the variation of the water-plane area. The results are calculated in regular wave states with a wave height of 1.0 m, and the RMS of the PTO force limit is 10 kN.

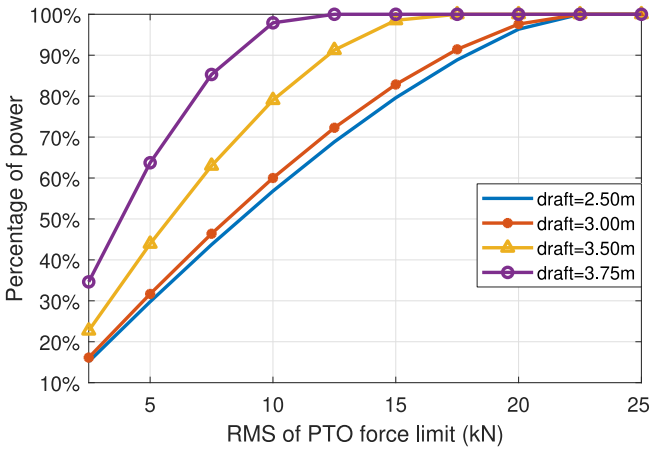

(a) Percentage of PTO absorbed power with force limits to that without force limits

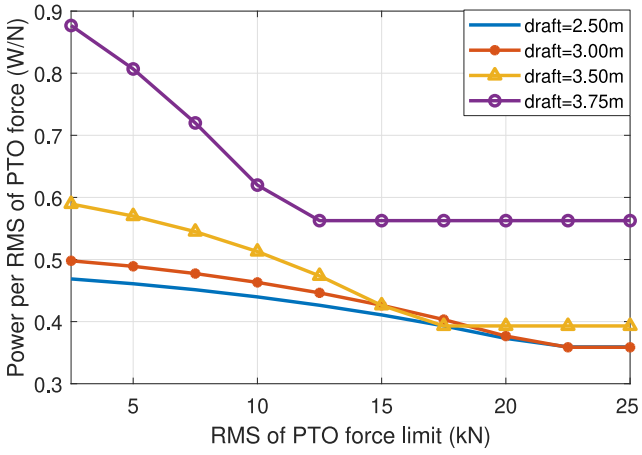

(b) PTO absorbed power per RMS of PTO force

Fig. 15. The influence of PTO force limits on the power performance. The results are calculated in a regular wave state with the wave height of 1.0 m and the wave period of 5.0 s.

decreases with the PTO force limit. However, an obvious difference can be observed with regard to the buoy draft of 3.75 m. In the nonlinear time domain analysis, its absorbed power per RMS of the PTO force is higher than that in the frequency domain analysis. Specifically, the ultimate value stays at approximately 0.58 W/N in the nonlinear time domain analysis, but it is nearly 0.5 W/N in the frequency domain analysis. This can be supported by the fact explained in Section 4.2.1 that the nonlinear components shifted its natural frequency to around 5.0 s. As a consequence, the power estimated by nonlinear time domain modeling is higher than the one obtained by the frequency domain analysis at this concerned wave period.

4.2.3. Performance comparison between the adjustable draft WEC and the fixed draft WEC

- *In regular waves*

  The absorbed power of the adjustable draft WEC is calculated by the nonlinear time domain model for regular wave conditions, as shown in Fig. 16. For comparison, the power performance of the semi-submerged fixed draft WEC is also presented in the figure. The calculation is performed based on the regular wave state with a wave height of 1.0 m, and the RMS of the PTO force limit is set as 10 kN. It can be seen from Fig. 16 that the adjustable draft WEC could absorb higher power over a range of wave periods. The gain of the power resulting from the adjustable draft system is mainly observed from the wave period of 3.5 s to 6.5 s. For instance, the highest power for the adjustable draft WEC is around 7 kW at the period of 4.0 s while it is only around 5.5 kW for the fixed draft WEC. The improvement is as high as 27%. When the wave period is below 4.0 s or above 6.5 s, the adjustable draft WEC and the fixed draft WEC tend to absorb the similar amount of power.

  Fig. 17 shows the adjusted drafts for the maximum delivered power in different wave periods. It is clear that the draft selection is strongly dependent on the wave period. The trend of the optimal draft is generally to first increase with the wave period and then to be relatively constant. This is because the natural period of the buoy increase with the buoy draft, which has been depicted in Fig. 2. At their natural periods, the larger drafts are associated with higher values of the RAO as well as higher buoy velocities. When the PTO force constraint starts to be a limiting factor of the power absorption, the higher velocity could contribute to the increase of the power absorption.

  Fig. 18 shows the ratios of the power absorbed by the adjustable draft WEC to that by the fixed draft WEC. The calculation is performed based on regular wave states with a wave height of 1.0 m. The corresponding ratios of power absorption in Fig. 18 is generally lower than those predicted by the frequency domain modeling, shown in Fig. 18. For instance, when the RMS of

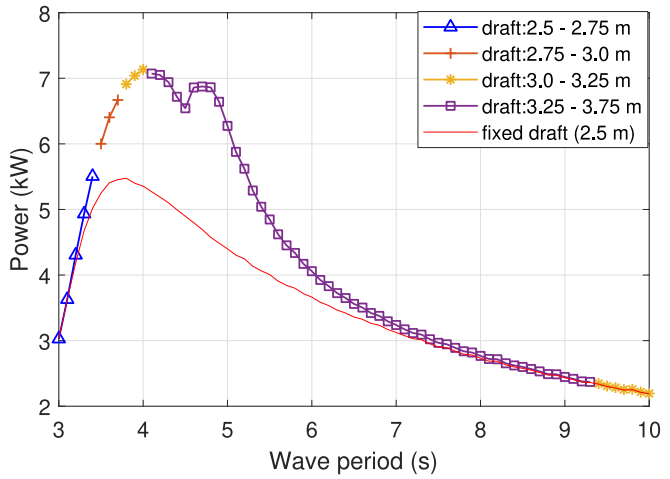

Fig. 16. Comparison between the power absorbed by the adjustable draft WEC and that by the WEC with a fixed draft of 2.5 m, and the considered wave height is 1.0 m and the RMS of the PTO force limit is 10 kN.

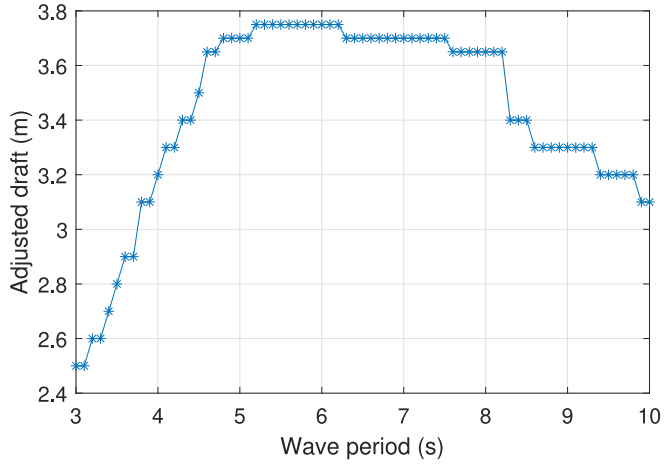

Fig. 17. The adjusted buoy drafts corresponding to the highest power for different wave periods, and the wave height is 1.0 m and RMS of the PTO force limit is 10 kN.

the PTO force limit is 10 kN, the highest ratio reaches 3.5 in Fig. 10 while it declines to around 1.45 in Fig. 18. However, even with considering nonlinear forces including the drag force, the adjustable draft WEC still suggests an obvious improvement of the power absorption, and the improvement is more significant when the PTO force limit becomes stricter. For example, when the RMS of the PTO force limit is 10 kN, the absorbed power of the adjustable draft WEC is 1.45 times that of the fixed draft WEC at the wave periods around 5.0 s. But it is only around 1.15 and 1.1 times as the RMS of the PTO force limit increases to 15 kN and 20 kN respectively. Therefore, it suggests that the adjustable draft system could improve the power performance of the spherical heaving point absorber in regular wave states, especially with the downsized PTO capacities.

- *In irregular waves*

  The power performance of the adjustable draft WEC and the fixed draft WEC in irregular wave states is calculated, shown in Fig. 19. As the simulation with irregular waves is run ten times for each case using different seeds, the mean values and error bar of the estimated power are presented. It can be seen that the power improvement resulting from the adjustable draft system in

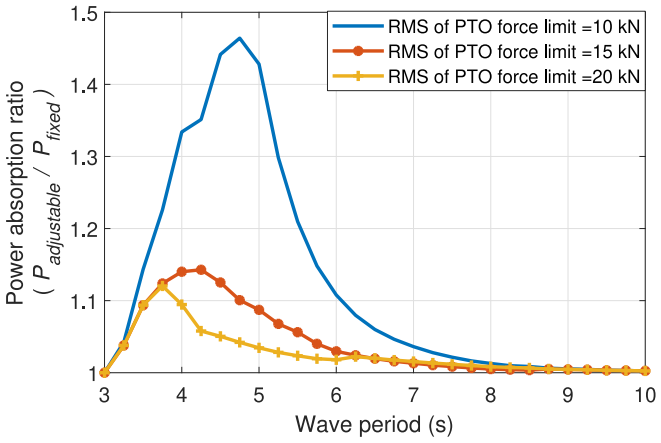

Fig. 18. Ratio of the power absorbed by the adjustable draft WEC to that by the fixed draft WEC in different RMS of the PTO force limit. The results are calculated in regular waves with a wave height of 1.0 m. $P_{adjustable}$ and P_{fixed} embody the power absorbed by the adjustable draft WEC and the power absorbed by the WEC with a fixed draft of 2.5 m.

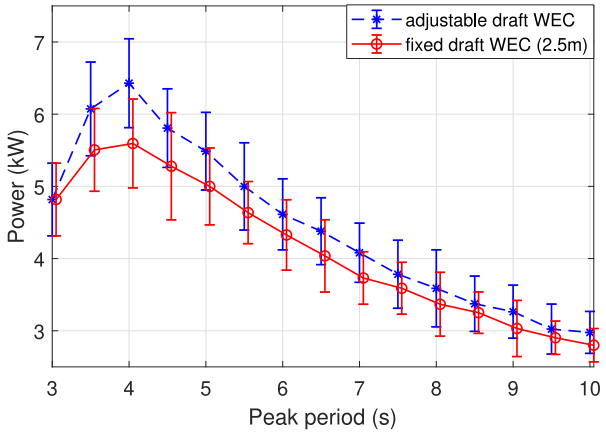

Fig. 19. Comparison between the power absorbed by the adjustable draft WEC and that by the WEC with a fixed draft of 2.5 m, and the considered significant wave height is 1.5 m and the RMS of the PTO force limit is 10 kN.

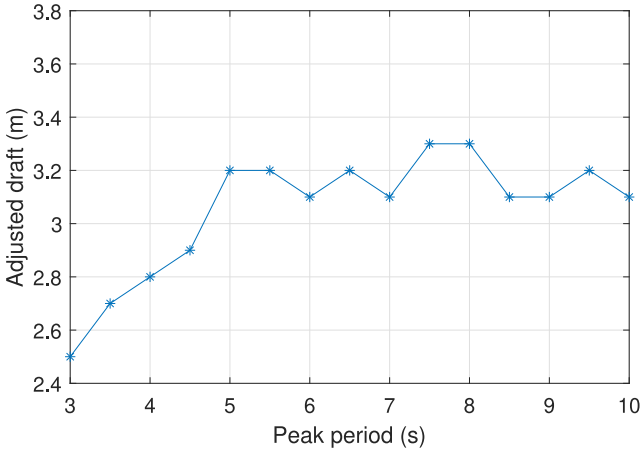

Fig. 20. The adjusted buoy drafts corresponding to the highest power for different wave periods, and the considered significant wave height is 1.5 m and the RMS of the PTO force limit is 10 kN.

irregular waves is less noticeable than the results from regular waves. The reason is that increasing the buoy draft reduces the

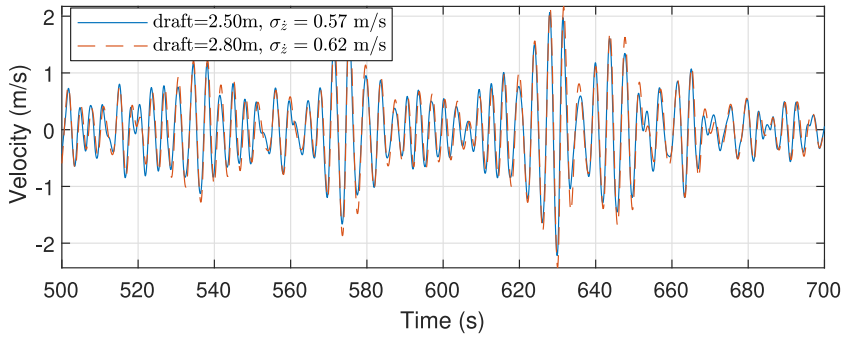

(a) Velocity

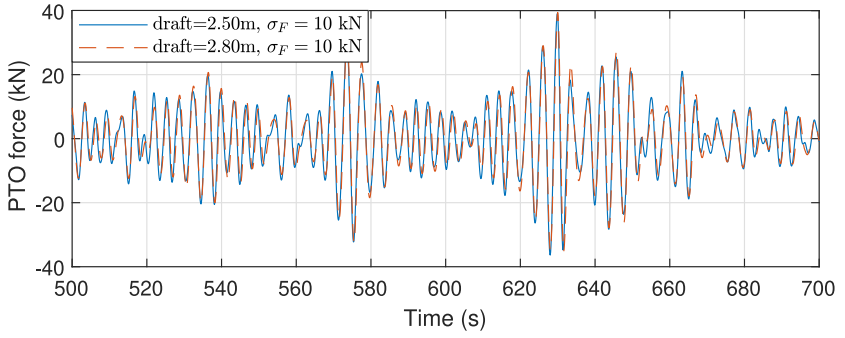

(b) PTO force

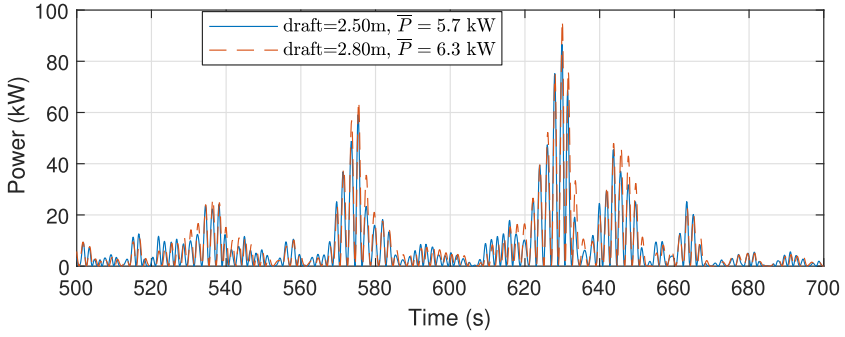

(c) Power

Fig. 21. The time domain responses of the buoy with the draft of 2.5 m and 2.8 m, corresponding to the wave elevation as input. The simulation is performed based on an irregular wave state with a significant wave height of 1.5 m and peak period of 4.0 s. The PTO damping is optimized subjected to the force constraints of RMS of 10 kN, with the values of 17600 kg/s and 16200 kg/s for the buoy draft of 2.5 m and 2.8 m. $\sigma_{\dot{z}}$ and σ_F embody the standard deviation of the velocity and PTO force.

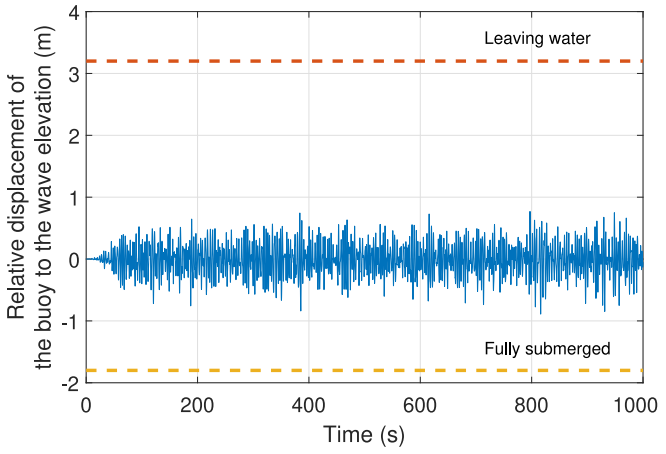

Fig. 22. The relative displacement of the buoy to the wave elevation, and the buoy draft is adjusted to 3.2 m. The results are calculated in an irregular wave state with a significant wave height of 1.5 m and peak period of 5.0 s, and the RMS of the PTO force limit is 10 kN.

absorption bandwidth of the buoy, and the narrower bandwidth reflects the incapability to respond to broad wave frequencies other than the natural frequency. Although the power absorption of the buoy with larger drafts in irregular waves is relatively weakened with regard to that in regular wave states, there is still power improvement resulting from the application of the adjustable draft system. For instance, the highest mean values of the absorbed power for the fixed draft WEC and adjustable draft WEC are approximately 5.7 and 6.4 kW, and the improvement is around 12%. In addition, it is observed that the gain of power absorption is mainly located between the peak periods of 4.5 and 6.0 s. When the peak period is above 7.0 s, the difference between the power absorption of the adjustable draft WEC and the fixed draft WEC is negligible. One possible approach to improve the power performance of this concept in irregular waves is to optimize the buoy geometry, by which the issue of narrow absorption bandwidth is expected to be mitigated. As indicated by Anon (2016), the absorption bandwidth increases with the resistive term, and thus the buoy geometries with the radiation damping increasing with the draft might be desirable.

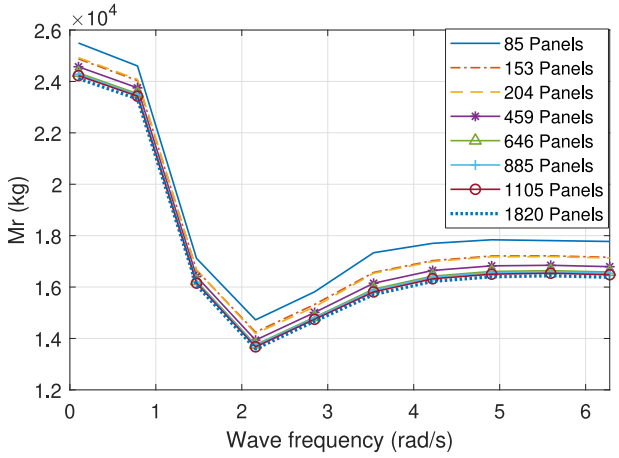

Fig. A.23. Mesh convergence analysis of Nemoh with regard to the added mass coefficients of the considered heaving spherical buoy with a buoy draft of 3.0 m.

The adjusted buoy drafts corresponding to the maximum power absorption for different peak periods in irregular wave states are shown in Fig. 20. The tendency of the adjusted draft with the peak period is first to increase and then to be stabilized at around 3.2 m in spite of the small fluctuations. Comparing the results with the draft adjustment in regular waves from Fig. 17, the values of the adjusted draft in irregular waves are accordingly lower. For instance, the adjusted draft in regular waves is higher than 3.6 m for the wave period between 4.5 and 8.2 s, while the largest adjusted draft is 3.3 m in irregular waves. This is also because the larger buoy drafts have a narrower bandwidth, which penalizes its power absorption in irregular waves.

As suggested in Fig. 20, the adjusted buoy draft is 2.8 m for the peak period of 4.0 s. Thus, the instantaneous responses of the WEC with the buoy drafts of 2.5 and 2.8 m are depicted in Fig. 21 to represent the performance of the adjustable draft WEC and fixed draft WEC. For a fair comparison, the generated profile of the wave elevation is maintained identical for these two buoy drafts in the simulation. It can be seen from Fig. 21(a) and (b) that the buoy draft of 2.8 m is generally related to higher velocities than that of 2.5 m at the same PTO force constraint. Therefore, the power absorbed by the buoy draft of 2.8 m is accordingly higher, as shown in Fig. 21(c).

As the buoy draft increases, the possibility of the buoy being fully submerged could be higher. As a consequence, the prediction accuracy of the power performance would decrease, since the effect is not considered in the numerical model. To justify the accuracy of the performance identification, the instantaneous relative displacement of the buoy to the wave elevation is calculated for an adjusted buoy draft, shown in Fig. 22. The adjusted buoy draft of 3.2 m in the peak period of 5.0 s is considered as a particular case. This case is sufficiently representative since the relative displacement is rather high at the wave periods between 3.5 and 5.0 s (shown in 13), and the buoy draft of 3.2 m is almost the largest value used in the irregular wave states (shown in Fig. 22). It is observed from Fig. 22 that the relative displacement hardly gets close to the two values indicating the cases of leaving water or being fully submerged within a simulation time duration of 1000 s. Thus, the current model is thought to be verified for the considered simulation cases in the time domain analysis. However, it should be realized that the possibility of the occurrence could increase if higher wave heights are considered, and then the accuracy of the current model would be challenged.

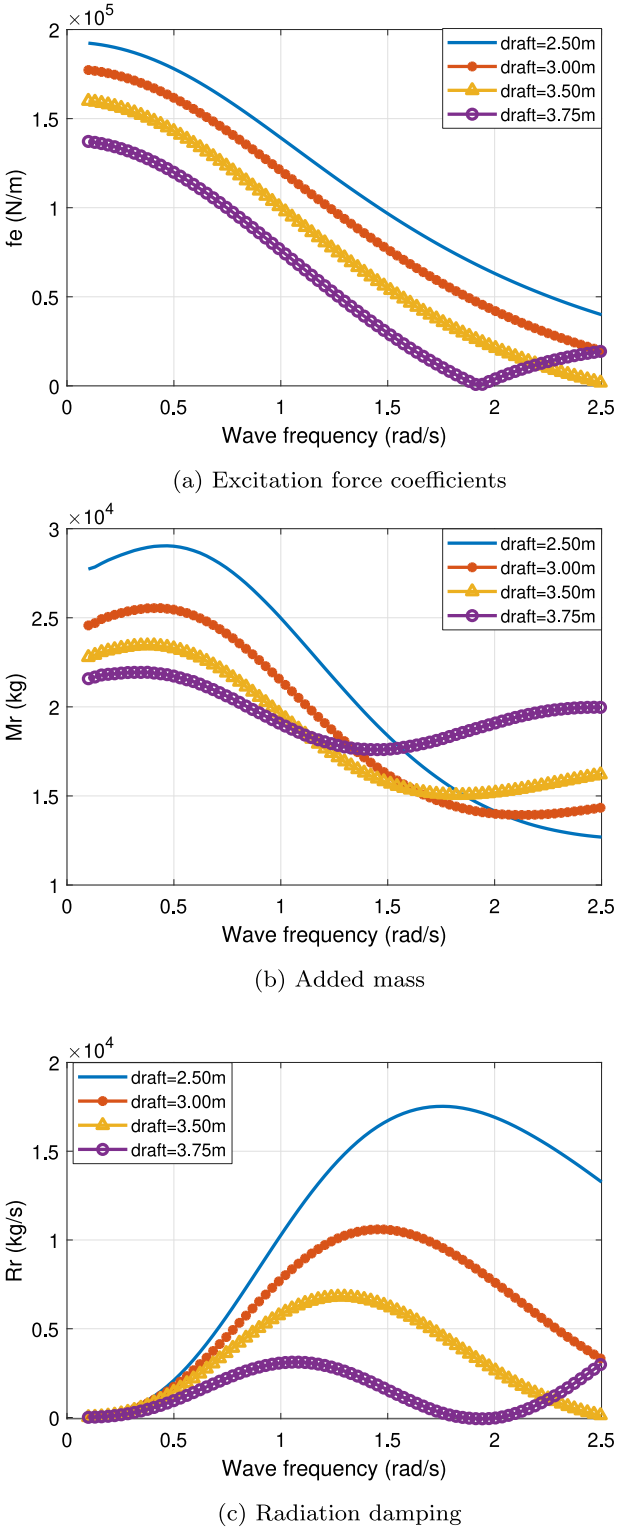

Fig. B.24. Hydrodynamic coefficients of the floating buoy in heaving for different buoy drafts.

5. Summary and conclusion

In this paper, an adjustable draft system is proposed for the heaving point absorber concept. By means of this system, the buoy draft can be adapted to the wave state. First, the proposed system and the considered WEC concept are described. Next, a frequency domain model is

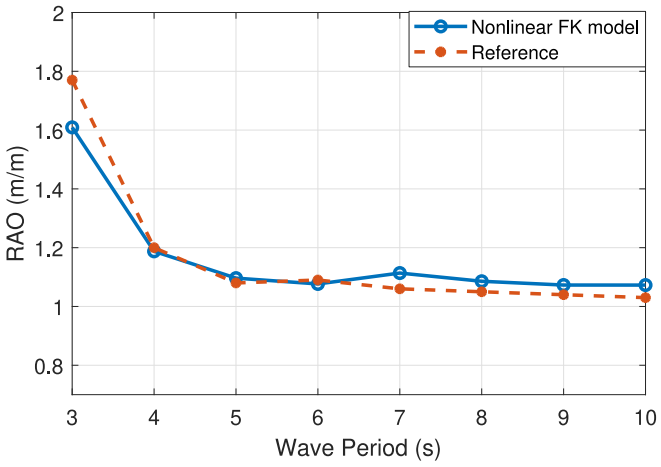

Fig. C.25. RAO obtained from the reproduced model and the Giorgi and Ringwood (2017b).

established to study the effect of the draft adjustment on performance of the WEC. The power performance of the adjustable draft WEC and the fixed draft WEC are compared for different PTO force constraints considerations. Furthermore, to take into account the nonlinear forces, an algebraic nonlinear time domain model is used to re-evaluate the performance of the WEC integrated with the adjustable draft system, in which both regular waves and irregular waves are considered. Based on the results, the following concluding remarks are drawn.

Firstly, the draft adjustment of the spherical buoy has a significant influence on its hydrodynamic coefficients in heave mode. The excitation force can be reduced by increasing the buoy draft. The larger buoy drafts correspond to the higher peak value of the heave RAOs but the narrower bandwidth. However, this conclusion is limited to the spherical floating buoy geometry, and the dependence of the hydrodynamic performance on the draft adjustment would differ with the buoy geometry. It is therefore recommended to conduct further investigation on the relevance of the buoy geometry to the performance of the adjustable draft system.

Secondly, the PTO force amplitude and average power of WECs are highly related to the buoy draft. Adapting the buoy draft to wave states makes it possible to control the required PTO force. The required PTO force can be reduced by increasing the buoy draft. Therefore the adjustable draft system can be used to implement the downsizing of PTO capacity.

Thirdly, the buoy draft adjustment varies the natural frequency of the WEC, and thus adapting the buoy draft to wave states could improve the power absorption. Reasonably adjusting the buoy draft is able to mitigate the negative effect of PTO force constraints on power performance. In addition, the performance of the adjustable draft system is related to the buoy size, and the wave periods when the power absorption can be clearly gained is increased by scaling the buoy up. Furthermore, nonlinear forces could make a difference to power absorption of the WEC, and the power absorption from the nonlinear model is remarkably lower than that estimated in the frequency domain analysis at the resonance regions. With regard to the fixed draft WEC, the application of the adjustable draft system is able to improve the power performance of a spherical point absorber, especially in the cases with the downsized PTO capacities. In the considered regular wave states, the power absorption could be improved around 27% in particular cases. In irregular wave states, less power improvement is observed since the absorption bandwidth is relatively narrowed by the increase of the buoy draft. Nevertheless, in the considered irregular wave conditions, the power absorption can be improved by approximately 12% in particular wave state.

CRediT authorship contribution statement

Jian Tan: Conception and design of study, Acquisition of data, Analysis and/or interpretation of data, Writing – original draft, Writing – review & editing. **Henk Polinder:** Conception and design of study, Writing – original draft. **Antonio Jarquin Laguna:** Conception and design of study, Analysis and/or interpretation of data, Writing – original draft, Writing – review & editing. **Sape Miedema:** Conception and design of study, Writing – original draft.

Declaration of competing interest

The authors declare that they have no known competing financial interests or personal relationships that could have appeared to influence the work reported in this paper.

Acknowledgments

The authors wish to thank offshore dredging engineering (ODE) group in Delft University of Technology for supporting the Ph.D. project relating to this research. The authors would like to thank Dr. Giuseppe Giorgi for his suggestion regarding the nonlinear algebraic Froude–krylov model. The authors also would like to thank Prof. John Ringwood for providing highly valuable comments and advice on our initial work, which helped us to improve the concept design. All authors approved the version of the manuscript to be published.

Funding

This research has received funding from China Scholarship Council under Grant: 201806950003.

Appendix A. Convergence verification of hydrodynamic calculation

A mesh convergence study is performed to verify the hydrodynamic results calculated by Nemoh. As an example, Fig. A.23 depicts the influence of the number of panels in the mesh on the prediction of the added mass coefficients of the heaving buoy with a buoy draft of 3.0 m. It is observed that the difference among mesh solutions with more than 646 panels is negligible. However, it is known that the computational time increases with the number of panels. To achieve a compromise between the accuracy and computational loads, the number of panels is maintained between 700 and 900 when calculating the hydrodynamic coefficients of the buoy with different buoy drafts.

Appendix B. The hydrodynamic coefficients for different buoy drafts

See Fig. B.24.

Appendix C. The verification of the reproduced nonlinear time domain model

To verify the reproduced nonlinear Froude–Krylov time domain model, a comparison is made between RAOs estimated by the reproduced model and referred to Giorgi and Ringwood (2017b). As in Giorgi and Ringwood (2017b), the calculation is performed for the buoy with a draft of 2.50 m, and the wave steepness is 0.018. As is shown in Fig. C.25, a good agreement between the reproduced model and the reference is observed. In this RAO comparison, the viscous force and Wheeler stretching correction are not considered in the reproduced model, which is intended to maintain consistency with the model reported in the Giorgi and Ringwood (2017b). Thus, it can be concluded that this nonlinear time domain model is reformulated correctly in the present paper.

References

Aderinto, T., Li, H., 2018. Ocean wave energy converters: Status and challenges. Energies 11 (5), 1–26.

Al Shami, E., Wang, X., Zhang, R., Zuo, L., 2019. A parameter study and optimization of two body wave energy converters. Renew. Energy 131, 1–13.

Anon, 2016. Numerical Modelling of Wave Energy Converters.

Babarit, A., Delhommeau, G., 2015. Theoretical and numerical aspects of the open source BEM solver NEMOH. In: 11th European Wave and Tidal Energy Conference (EWTEC2015).

Babarit, A., Hals, J., Muliawan, M.J., Kurniawan, A., Moan, T., Krokstad, J., 2012. Numerical benchmarking study of a selection of wave energy converters. Renew. Energy 41, 44–63.

Backer, G., 2009. Hydrodynamic Design Optimization of Wave Energy Converters Consisting of Heaving Point Absorbers. Ghent University, Belgium, pp. 1–3.

Cahill, B., Lewis, A.W., 2014. Wave period ratios and the calculation of wave power. In: The 2nd Marine Energy Technology Symposium. pp. 1–10.

Cummins, W., Iiuhl, W., Uinm, A., 1962. The Impulse Response Function and Ship Motions. Citeseer.

De Andres, A., Medina-Lopez, E., Crooks, D., Roberts, O., Jeffrey, H., 2017. On the reversed LCOE calculation: Design constraints for wave energy commercialization. Int. J. Mar. Energy 18, 88–108.

Falnes, J., 2003. Ocean waves and oscillating systems. In: Ocean Engineering. Vol. 30, (7), p. 953.

Giorgi, G., Ringwood, J.V., 2017a. Consistency of viscous drag identification tests for wave energy applications. In: 12th European Wave and Tidal Energy Conference. pp. 1–8.

Giorgi, G., Ringwood, J.V., 2017b. Computationally efficient nonlinear Froude–Krylov force calculations for heaving axisymmetric wave energy point absorbers. J. Ocean Eng. Mar. Energy 3 (1), 21–33.

Giorgi, G., Ringwood, J.V., 2017c. Nonlinear Froude-Krylov and viscous drag representations for wave energy converters in the computation/fidelity continuum. Ocean Eng. 141 (January), 164–175.

Giorgi, G., Sirigu, S., Bonfanti, M., Bracco, G., Mattiazzo, G., 2021. Fast nonlinear Froude–Krylov force calculation for prismatic floating platforms: a wave energy conversion application case. J. Ocean Eng. Mar. Energy 7 (4), 439–457.

Guo, B., Patton, R., Jin, S., 2017. Identification and validation of excitation force for a heaving point absorber wave energy convertor. In: 12th European Wave and Tidal Energy Conference. pp. 1–6.

Hals, J.A.r., Bjarte-Larsson, T., Falnes, J., 2002. Optimum reactive control and control by latching of a wave-absorbing semisubmerged heaving sphere. In: 21st International Conference on Offshore Mechanics and Arctic Engineering. (January), pp. 415–423. http://dx.doi.org/10.1115/omae2002-28172.

Kurniawan, A., Moan, T., 2013. Optimal geometries for wave absorbers oscillating about a fixed axis. IEEE J. Ocean. Eng. 38 (1), 117–130.

Lawson, M., Yu, Y.-H., Nelessen, A., Ruehl, K., Michelen, C., 2014a. Implementing nonlinear buoyancy and excitation forces in the wec-sim wave energy converter modeling tool. In: International Conference on Offshore Mechanics and Arctic Engineering. Vol. 45547, American Society of Mechanical Engineers, V09BT09A043.

Lawson, M., Yu, Y.-H., Ruehl, K., Michelen, C., et al., 2014b. Development and demonstration of the WEC-sim wave energy converter simulation tool.

Lehmann, M., Karimpour, F., Goudey, C.A., Jacobson, P.T., Alam, M.R., 2017. Ocean wave energy in the United States: Current status and future perspectives. Renew. Sustain. Energy Rev. 74 (February 2016), 1300–1313.

Payne, G., 2008. Guidance for the experimental tank testing of wave energy converters. SuperGen Mar..

Penalba, M., Giorgi, G., Ringwood, J.V., 2017a. Mathematical modelling of wave energy converters: A review of nonlinear approaches. Renew. Sustain. Energy Rev. 78 (August 2015), 1188–1207.

Penalba, M., Kelly, T., Ringwood, J., 2017. Using NEMOH for modelling wave energy converters : A comparative study with WAMIT. In: 12th European Wave and Tidal Energy Conference. p. 10.

Penalba Retes, M., Giorgi, G., Ringwood, J., 2015. A review of non-linear approaches for wave energy converter modelling. In: Proceedings of the 11th European Wave and Tidal Energy Conference. European Wave and Tidal Energy Conference 2015.

Pérez, T., Fossen, T., 2008. Time-vs. frequency-domain identification of parametric radiation force models for marine structures at zero speed. Model. Identif. Control 29 (1), 1–19.

Prado, M., Polinder, H., 2013a. Direct Drive Wave Energy Conversion Systems: An Introduction. Woodhead Publishing Limited, pp. 175–194.

Prado, M., Polinder, H., 2013b. Direct drive wave energy conversion systems: An introduction. Electr. Drives Direct Drive Renew. Energy Syst. 175–194.

Sergiienko, N.Y., Cazzolato, B.S., Ding, B., Hardy, P., Arjomandi, M., 2017. Performance comparison of the floating and fully submerged quasi-point absorber wave energy converters. Renew. Energy 108, 425–437.

Sergiienko, N.Y., Rafiee, A., Cazzolato, B.S., Ding, B., Arjomandi, M., 2018. Feasibility study of the three-tether axisymmetric wave energy converter. Ocean Eng. 150 (December 2017), 221–233.

Shadman, M., Estefen, S.F., Rodriguez, C.A., Nogueira, I.C., 2018. A geometrical optimization method applied to a heaving point absorber wave energy converter. Renew. Energy 115, 533–546.

Shek, J., Macpherson, D., Mueller, M., 2008. Phase and amplitude control of a linear generator for wave energy conversion. In: 4th IET International Conference on Power Electronics, Machines and Drives (PEMD 2008). pp. 66–70. http://dx.doi.org/10.1049/cp:20080484.

Stallard, T.J., Weller, S.D., Stansby, P.K., 2009. Limiting heave response of a wave energy device by draft adjustment with upper surface immersion. Appl. Ocean Res. 31 (4), 282–289.

Tai, V.C., See, P.C., Merle, S., Molinas, M., 2012. Sizing and control of the electric power take off for a buoy type point absorber wave energy converter. Renew. Energy Power Q. J. 1 (10), 1614–1619.

Tan, J., Polinder, H., Laguna, A.J., Miedema, S., 2022. The application of the spectral domain modeling to the power take-off sizing of heaving wave energy converters. Appl. Ocean Res. 122, 103110.

Tan, J., Polinder, H., Laguna, A.J., Wellens, P., Miedema, S.A., 2021a. The influence of sizing of wave energy converters on the techno-economic performance. J. Mar. Sci. Eng. 9 (1), 52.

Tan, J., Polinder, H., Wellens, P., Miedema, S., 2020. A feasibility study on downsizing of power take off system of wave energy converters. In: Developments in Renewable Energies Offshore: Proceedings of the 4th International Conference on Renewable Energies Offshore (RENEW 2020, 12-15 October 2020, Lisbon, Portugal). CRC Press, p. 140.

Tan, J., Wang, X., Jarquin Laguna, A., Polinder, H., Miedema, S., 2021b. The influence of linear permanent magnet generator sizing on the techno-economic performance of a wave energy converter. In: 2021 13th International Symposium on Linear Drives for Industry Applications (LDIA). pp. 1–6. http://dx.doi.org/10.1109/LDIA49489.2021.9505880.

Tedeschi, E., Carraro, M., Molinas, M., Mattavelli, P., 2011. Effect of control strategies and power take-off efficiency on the power capture from sea waves. IEEE Trans. Energy Convers. 26 (4), 1088–1098.

Tedeschi, E., Molinas, M., 2010a. Wave-to-Wave Buoys Control for Improved Power Extraction under Electro-Mechanical Constraints. (1), IEEE.

Tedeschi, E., Molinas, M., 2010b. Impact of control strategies on the rating of electric power take off for wave energy conversion. In: IEEE International Symposium on Industrial Electronics. (February 2019), pp. 2406–2411. http://dx.doi.org/10.1109/ISIE.2010.5637522.

Tedeschi, E., Molinas, M., 2012. Tunable control strategy for wave energy converters with limited power takeoff rating. IEEE Trans. Ind. Electron. 59 (10), 3838–3846.

Tokat, P., Thiringer, T., 2018. Sizing of IPM generator for a single point absorber type wave energy converter. IEEE Trans. Energy Convers. 33 (1), 10–19.

Wang, L., Lin, M., Tedeschi, E., Engström, J., Isberg, J., 2020. Improving electric power generation of a standalone wave energy converter via optimal electric load control. Energy 211, 118945.

Wang, L., Ringwood, J.V., 2021. Control-informed ballast and geometric optimisation of a three-body hinge-barge wave energy converter using two-layer optimisation. Renew. Energy 171, 1159–1170.

Wang, L., Zhao, T., Lin, M., Li, H., 2022. Towards realistic power performance and techno-economic performance of wave power farms: The impact of control strategies and wave climates. Ocean Eng. 248, 110754.

Wen, Y., Wang, W., Liu, H., Mao, L., Mi, H., Wang, W., Zhang, G., 2018. A shape optimization method of a specified point absorber wave energy converter for the South China Sea. Energies 11 (10).